JOURNAL OF THE ROYAL SOCIETY Interface

Spectrally resolved fluorescent lifetime imaging

Quentin S Hanley

J. R. Soc. Interface 2009 **6**, S83-S92
doi: 10.1098/rsif.2008.0393.focus

Interface focus

J. R. Soc. Interface (2009) **6**, S83–S92
doi:10.1098/rsif.2008.0393.focus
Published online 2 December 2008

REVIEW

Spectrally resolved fluorescent lifetime imaging

Quentin S. Hanley*

School of Science and Technology, Nottingham Trent University, Clifton Lane, Nottingham NG11 8NS, UK

Placing an imaging spectrograph or related components capable of generating a spectrum between a microscope and the image intensifier of a conventional fluorescence lifetime imaging (FLIM) system creates a spectrally resolved FLIM (SFLIM). This arrangement provides a number of opportunities not readily available to conventional systems using bandpass filters. The examples include: simultaneous viewing of multiple fluorophores; tracking of both the donor and acceptor; and observation of a range of spectroscopic changes invisible to the conventional FLIM systems. In the frequency-domain implementation of the method, variation in the fractional contributions from different fluorophores along the wavelength dimension can behave as a surrogate for a frequency sweep or spatial variations while analysing fluorophore mixtures. This paper reviews the development of the SFLIM method, provides a theoretical and practical overview of frequency-domain SFLIM including: presentation of the data; manifestations of energy transfer; observation of multiple fluorophores; and the limits of single frequency methods.

Keywords: fluorescent; imaging; frequency methods

1. INTRODUCTION

The first spectrally resolved FLIM (SFLIM) system (figure 1; Vereb *et al.* 1998) was a time-domain instrument designed to measure lifetimes on the millisecond time scale and applied to the analysis of lanthanide chelate crystals. It operated as a detection system for a single line within the sample corresponding to the location, where the sample image coincided with the entrance slit of the spectrograph. This basic design, consisting of a spectral dispersion element introduced into the detection path of a lifetime imaging system, has been used in a variety of forms in both the time and frequency domains (Hanley *et al.* 2002; Bird *et al.* 2004; Tramier *et al.* 2004; Hanley & Ramkumar 2005; Forde & Hanley 2006; Pelet *et al.* 2006; Yan *et al.* 2006; De Beule *et al.* 2007; Rück *et al.* 2007). In these implementations, a number of advantages have been noted including: the ability to observe the donor and acceptor simultaneously (Hanley *et al.* 2002; Tramier *et al.* 2004; Pelet *et al.* 2006); the capability to better understand the fluorophores in a mixture (Yan *et al.* 2006); and the possibility of sorting out complex native fluorescence without *a priori* knowledge of the sample (De Beule *et al.* 2007).

In addition to this body of work in which a wavelength axis is generated with the assistance of a dispersion element, parallel developments have taken place using filters. In this parallel body of work, filters are used to develop lifetime images corresponding to different wavelength bands (Tinnefeld *et al.* 2001; Knemeyer *et al.* 2003, 2007). The work of this group uses the same acronym, key words and slightly precedes the published use of 'SFLIM' to describe a system with spectral selection using a dispersion element. To rectify this confusion, an attempt was made to introduce imaging spectroscopic fluorescence lifetime imaging (ISFLIM) as an alternative (Forde & Hanley 2006; Hanley *et al.* 2006). As this refers to only a subset of SFLIM methods, it is unlikely to find widespread use. A time-correlated single photon counting technique with a 16 channel multianode photo-multiplier tube and a spectrograph has been described. This is also called SFLIM and has been given the acronym SLIM (Rück *et al.* 2007). It is important to note that the motivation for the techniques bearing the SFLIM and SLIM acronyms is similar: to provide additional information from the spectral characteristics of fluorophores to ease the interpretation of a complex sample. Users and developers of the systems employing dispersion elements should be aware of the speed advantages of filter-based systems, while users employing filters may find a discussion of the benefits of large numbers of spectral segments helpful. This paper is primarily concerned with the latter issue.

Despite considerable interest, SFLIM remains an underused tool. Its potential has not been fully realized in studies of biological systems and, when compared

*quentin.hanley@ntu.ac.uk

One contribution of 9 to a Theme Supplement 'Quantitative fluorescence microscopy: The 1st international Theodor Förster lecture series'.

Received 10 September 2008
Accepted 13 November 2008

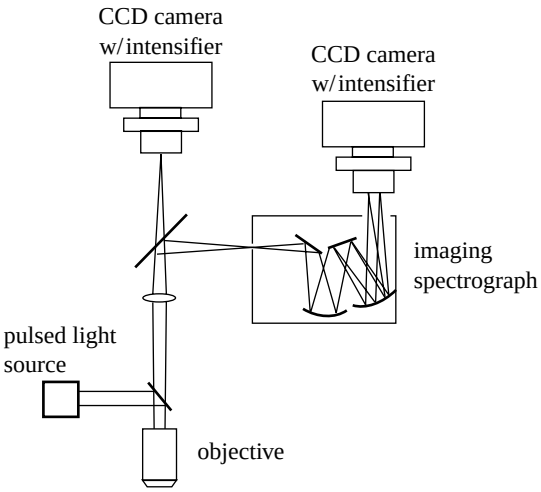

Figure 1. The first known SFLIM system as reported by Vereb *et al.* (1998). The SFLIM system was implemented with a grating-based imaging spectrograph, image intensifier and Xe flash lamp. Data were collected on the millisecond time scale from crystals composed of lanthanide chelates.

with a conventional FLIM, has remained largely of academic interest. There are many reasons for this. It is an unfamiliar format which in its current form cannot be easily understood by non-specialists. Dispersed systems are comparatively slow and there is an unavoidable trade-off between increasing the number of spectral elements to obtain more information and lowering the rate of acquisition. Tools to calibrate and validate SFLIM across the spectrum are limited and datasets are large and complex. This paper will explore the key features of SFLIM, the theory that underpins it and some of the unique opportunities it provides.

2. THEORY

2.1. Spectral images

One of the barriers to wider adoption of SFLIM is the unfamiliar format of spectral images. Spectral images are generated by a spectrograph that preserves the image quality along the slit axis while dispersing the incoming light along a second. In presenting such an image, the wavelength axis is usually portrayed along the x-axis and the slit direction along y. In this paper, we will describe this as an ordered triple (x, λ and I), with the designations x, λ and I referring to the first of three spatial dimensions, wavelength and intensity, respectively. While there are a variety of ways to generate such images, this type of spectral image has only a single spatial axis while samples have three-dimensional (x, y and z) structures. The normal view presented to a camera from a microscope is two-dimensional (x, y and I). As such, the simplest spectral image is somewhat restrictive in the portions of a sample it will interrogate. Systems for generating spectral images with two spatial dimensions (x, y, λ and I) have been described. These include imaging spectrographs combined with stage scanning, Hadamard (Hanley *et al.* 1999) and Fourier (Garini *et al.* 1996) multiplexed systems, tunable filters (Levenson 2006) and confocal laser scanning microscopes with microspectroscopic hardware (Rück *et al.* 2007). The latter three approaches are available commercially. Spectral images with three spatial dimensions (x, y, z, λ and I) have been reported (Hanley *et al.* 2000), and the ability to collect such images is available commercially as an option on some confocal microscopes. The five-dimensional output of such instruments is rarely published in detail but their flexibility is of a considerable value.

2.2. Frequency-domain fluorescence lifetimes

The frequency-domain method most commonly used for the measurement of lifetime images involves exciting a sample with a sinusoidally modulated light source, such as a laser (Marriott *et al.* 1991; Schneider & Clegg 1997; Esposito *et al.* 2005) or LED (Dinish *et al.* 2006; Elder *et al.* 2006), and detecting with a modulated detector. The most common implementation is the homodyne approach in which both excitation source and detector are modulated at the same frequency and a series of images are collected as the phase between light source and detector are shifted. The series of images are Fourier transformed or fit to a sinusoid and the modulation and phase of the emitted light computed (Gadella *et al.* 1994; Hanley *et al.* 2001). The measured modulation depth and phase shift between excitation and emission depends on the lifetime of the emitting species (Spencer & Weber 1969; Lakowicz 1999). From the phase and modulation depth two lifetime-related parameters may be computed,

$$\tau_\phi(x,\ y, z, \lambda, \omega) = \omega^{-1}\tan(\phi(x,\ y, z, \lambda)) \tag{2.1}$$

and

$$\tau_m(x,\ y, z, \lambda, \omega) = \omega^{-1}\sqrt{\frac{1}{m(x,\ y, z, \lambda)^2} - 1}, \tag{2.2}$$

where τ_ϕ is the phase lifetime; ω is $2\pi f$ (f is the frequency of modulation); ϕ is the phase shift between the excitation and the emitted light; τ_m is the modulation lifetime; and m is the modulation depth of the detected light.

The modulation depth and phase are predictable for a mixture of multiple fluorophores that do not undergo energy transfer or excited-state reactions (Weber 1981). A reasonably complete presentation involves three spatial dimensions, wavelength and frequency of modulation.

$$A(x,\ y, z, \lambda, \omega) = \frac{\sum_{i=1}^{n} \frac{\alpha_i(\lambda, x,\ y, z)\omega\tau_i^2}{1+\omega^2\tau_i^2}}{\sum_{i=1}^{n} \alpha_i(\lambda, x,\ y, z)\tau_i}, \tag{2.3}$$

$$B(x,\ y, z, \lambda, \omega) = \frac{\sum_{i=1}^{n} \frac{\alpha_i(\lambda, x,\ y, z)\tau_i}{1+\omega^2\tau_i^2}}{\sum_{i=1}^{n} \alpha_i(\lambda, x,\ y, z)\tau_i}, \tag{2.4}$$

$$\phi(x,\ y,\ z,\ \lambda,\ \omega) = \tan^{-1}\left(\frac{A(x,\ y,\ z,\ \lambda,\ \omega)}{B(x,\ y,\ z,\ \lambda,\ \omega)}\right) \tag{2.5}$$

and

$$m(x,\ y,\ z,\ \lambda,\ \omega) = \sqrt{A(x,\ y,\ z,\ \lambda,\ \omega)^2 + B(x,\ y,\ z,\ \lambda,\ \omega)^2}. \tag{2.6}$$

In these expressions, the α_i are the normalized pre-exponential factors. It is worth noting that ϕ and m are the polar coordinate representations of A and B. Equations (2.3)–(2.6) depend on three parameters: α_i, τ_i and ω. Each of these parameters has been used to solve a mixture. For example, lifetimes were systematically adjusted by quenching a mixture of rhodamine 6G and fluorescein (Hanley & Clayton 2005). Variation in α_i may occur spatially, spectrally or temporally, and this variation can be applied to the analysis of mixtures. Spatial-dependent (Verveer & Bastiaens 2003; Clayton *et al.* 2004) and wavelength-dependent (Hanley & Clayton 2005) variations in α_i have been employed to determine individual component lifetimes in a mixture. The author is not aware of temporal variations in α_i being applied to resolve a mixture. SFLIM is useful in this context because α_i varies with wavelength.

Similar equations are available for predicting the behaviour of mixtures in which excited-state reactions or energy transfer influence the results. A simplified approach to predicting m and ϕ for a fluorophore excited through Förster resonance energy transfer (FRET) and to crudely estimate the range of allowed mixing is given below; however, a detailed treatment of mixtures and energy transfer and excited-state processes is beyond the scope of this paper but can be found in the literature (Lakowicz & Balter 1982*a*,*b*; Forde & Hanley 2006).

2.3. Spectrum as a surrogate for frequency sweep

The goal of many types of lifetime imaging and analysis is the resolution of mixtures. These mixtures could range from two non-interacting fluorophores to complex multicomponent mixtures including energy transfer or excited-state reactions. When making measurements of complex mixtures in real samples, there is a compromise between the speed of acquisition, sample photobleaching and other factors. In the frequency-domain FLIM measurements, nearly all reported measurements are done at single frequencies. Multifrequency FLIM (Squire *et al.* 2000) has been described but is not widely used.

In SFLIM experiments, the practical restriction to single frequencies is less of a compromise since other parameters provide similar information. Equations (2.3)–(2.6) describe the dependence of m and ϕ on the parameters α, ω and τ. If these parameters vary sufficiently, a mixture of arbitrary complexity can be solved. Where systematic manipulation of any one parameter is possible or where one parameter varies across an image or set of images because of sample heterogeneity, that parameter can be used to solve a system of multiple fluorophores. Frequency provides nothing unique compared with α or τ. It is, however, easier to control systematically via hardware external to the sample. Careful selection and control of fluorophores to maximize variation in α combined with SFLIM can make a frequency sweep unnecessary.

2.4. *AB*-plots[1]

One approach to resolving binary mixtures is to plot the A and B parameters in an xy-coordinate system (Jameson *et al.* 1984; Clayton *et al.* 2004; Hanley & Clayton 2005). Pure, single-component lifetimes lie on a half-circle with a radius of 0.5 centred at (0.5, 0). From a set of measurements of m and ϕ, an *AB*-plot may be constructed directly in polar coordinates or in Cartesian coordinates after a simple transformation (Clayton *et al.* 2004; Hanley & Clayton 2005; Redford & Clegg 2005; Forde & Hanley 2006; Digman *et al.* 2008; Colyer *et al.* 2008).[2]

$$A(x,\ y,\ z,\ \lambda) = m(x,\ y,\ z,\ \lambda)\sin\phi(x,\ y,\ z,\ \lambda) \tag{2.7}$$

and

$$B(x,\ y,\ z,\ \lambda) = m(x,\ y,\ z,\ \lambda)\cos\phi(x,\ y,\ z,\ \lambda). \tag{2.8}$$

By determining the points where the line defined by mixing the two fluorophore lifetimes intersects the half-circle, the two lifetimes in a binary mixture can be determined. More specifically, let $A(x, y, z, \lambda) = u + vB(x, y, z, \lambda)$ be the line defined by a set of binary mixtures of two fluorophores. The two lifetimes composing the mixtures are

$$\tau_{1,2} = \frac{1 \pm \sqrt{1 - 4u(u+v)}}{2\omega u}. \tag{2.9}$$

More details of the derivation of this expression can be found in Clayton *et al.* (2004). The *AB*-plots are valuable in the context of SFLIM because they provide a convenient and robust (Hanley *et al.* 2005) space for presenting the results from SFLIM experiments, particularly those in which energy transfer occurs (Forde & Hanley 2006).

The *AB*-plots may be used to simplify a complex set of phase and modulation data (figure 2). The data shown are from a study of the interaction of propidium iodide (PI) with DNA (Hanley *et al.* 2002). PI is an intercalation dye similar to ethidium bromide (EB). Upon binding to the DNA, PI becomes more brightly fluorescent and the lifetime changes from short to long. The mechanism of this change is believed to be a

[1] *AB*-plots may now be found under a variety of names: *AB*-plots (Clayton *et al.* 2004) as is used here, polar plots (Redford & Clegg 2005) and phasor plots (Digman *et al.* 2008). The term '*AB*-plot' is used here to be consistent with earlier work; however, either of the other names is an accurate description. The equivalence of these diagrams to Cole–Cole plots in dielectric relaxation has been noted (Redford & Clegg 2005), and it might also be appropriate to consider them to be Argand diagrams. Of the three alternatives, polar plot is perhaps the best since it is simply the modulation and phase plotted in polar coordinates and as such may be most accessible to non-specialists. The first report of an *AB*-like plot in fluorescence dynamics used an S and G notation (Jameson *et al.* 1984). *ND* (Lakowicz 1999) and *PQ* (Lakowicz & Balter 1982*a*,*b*) notations may also be found in textbooks and the literature for related quantities.

[2] It should be noted that A and B may be computed directly from the raw data. It is not necessary to first compute the modulation and phase.

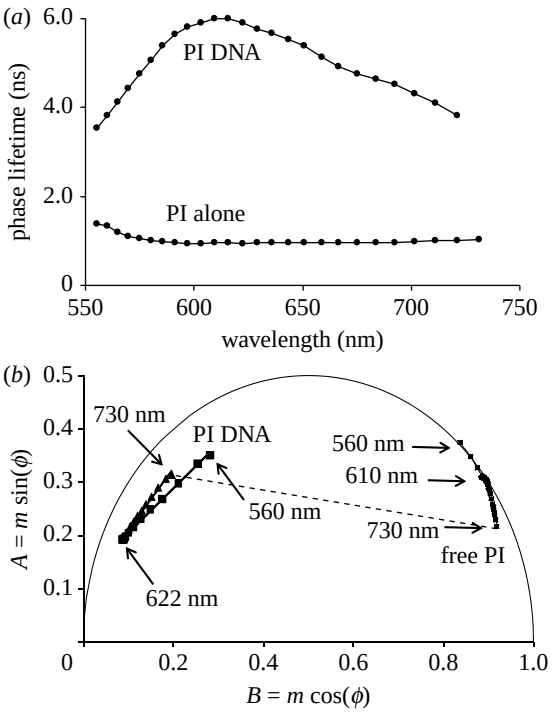

Figure 2. Comparison of the SFLIM data presented as either (*a*) lifetime spectra or (*b*) plotted in the *AB*-space. Data shown were collected on solutions of propidium iodide (PI) in the presence and the absence of DNA. These data clearly show the presence of at least three species in each of the samples. This is indicted by the three endpoints of the two line segments in each dataset (*b*) The striking feature which is very difficult to see clearly in (*a*) is that there is no evidence of a consistent mixing pattern between the two samples. An estimate of what such mixing would look like for a single wavelength is indicated by the dotted curves. Data adapted from Hanley *et al.* (2002).

dequenching process similar to EB (Olmsted & Kearns 1977; Jones *et al.* 1978; Leupin *et al.* 1985). These data (figure 2) were originally published as plots of phase and modulation lifetime spectra. However, the lifetime spectra were relatively uninformative (figure 2*a*). Based on the literature, a two-component model consisting of free and bound PI was applied to the data; however, no combination of the two non-interacting fluorophores explained the measurements. Eventually, an additional species was proposed in the green portion of the spectrum and a subsequent thin-layer chromatography confirmed the presence of a green fluorescing species. These effects would have been masked without the wavelength axis being present. Typical FLIM experiments would employ a single bandpass filter targeted to the emission maximum and this would exclude the wavelength-dependent variations in α. This study demonstrated the power of a single frequency SFLIM; however, conclusions related to the number of decay components could be reached only with difficulty.

Presenting the data in an *AB*-format (figure 2*b*) allows the presence of at least three species to be seen by inspection in both the presence and absence of DNA. Each line segment (figure 2*b*) represents two different fluorescent species. Most importantly, the dominant feature across the two samples shown is that there is no evidence of a trend between the free and bound samples. The dominant process is mixing between three species within each sample. A key point to be made about figure 2 is that the presentation of the SFLIM data as lifetime spectra is often uninformative. Often this information is presented more robustly and to greater interpretive effect in the *AB*-space. For many experiments, knowing the number of components present (e.g. does a sample contain free donor, a donor–acceptor and free acceptor or does it contain only free donor and free acceptor) is extremely valuable.

2.5. *Wavelength-modified AB*-plots

The PI data presented in §2.4 highlighted the value of having spectrally resolved lifetime measurements and the use of the *AB*-representation to aid qualitative interpretation of the SFLIM data. Indicating specific wavelength positions (figure 2*b*) helped to guide the interpretation. However, SFLIM experiments collect the data with a wavelength axis and collapsing this additional information, while useful for observing general trends, does not make full use of the available information. A more correct representation is to add a third axis. Such data (figure 3*a*) may be presented as a three-dimensional plot. The data show the time evolution of a photobleaching experiment in a system of multiple fluorophores undergoing energy transfer (Hanley *et al.* 2006) replotted to include the wavelength dependence of the data (figure 3*a*). While they remain complex, it is immediately clear that much of the data are relatively constant when observed with the wavelength axis preserved. The most interesting portions of the time series are readily apparent: early time points where the spectra lie outside the semicircle (indicative of energy transfer); portions of the spectrum greater than 650 nm (acceptor region); and where the data change rapidly with time (early time points and longer wavelength). The remainder of the data are found near (0.23 and 0.27) and between 540 and 650 nm (figure 3*a*). This is consistent with a system of multiple fluorophores dominated by energy transfer to a terminal acceptor in the red portion of the spectrum. Considering the amount of effort that goes into proofs of energy transfer, the ability to quickly interpret at this level of detail represents a significant advance.

2.6. *AB*-plots with frequency changes

Review of equations (2.3)–(2.6) shows that the frequency always appears as a multiplier of τ. The consequence of this is that changing ω has a similar effect on A and B to a change of lifetime. In the *AB*-format, variably quenched solutions producing single-component lifetimes track the arc of the semicircle (Hanley & Clayton 2005). As noted previously (Clayton *et al.* 2004), at a given frequency, all possible single-component lifetimes lie on the semicircle. Conversely, for a given single-component lifetime, measurements at any frequency will be restricted to a semicircle of radius 0.5 centred at (0.5, 0). Changing the modulation frequency induces a distribution in the

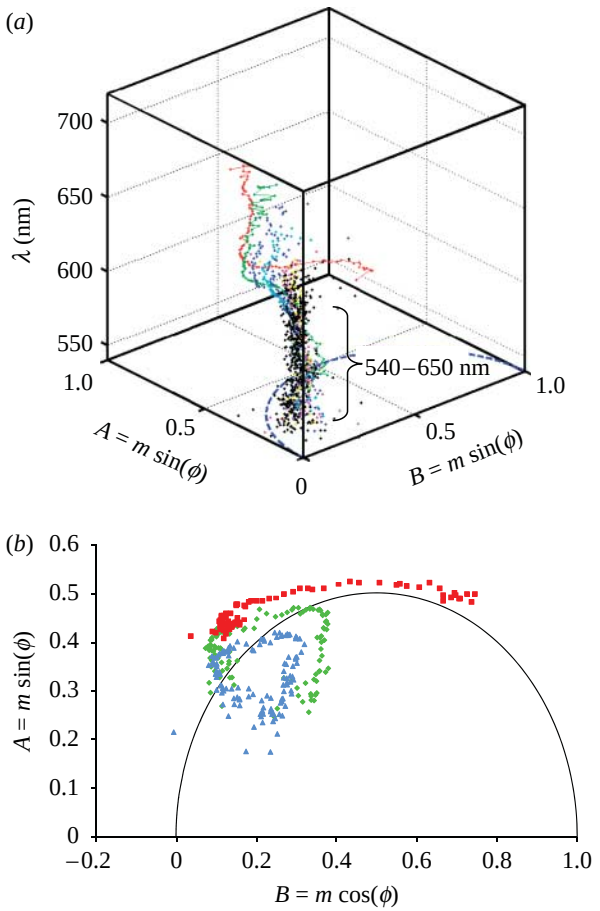

Figure 3. (*a*) Three-dimensional wavelength-dependent *AB*-plot of T-8883 beads collected during photobleaching with UV light and (*b*) data as in (*a*) showing data from 0, 20 and 40 min and projected along the wavelength axis. The red, green and blue markers correspond to the 0, 20 and 40 min time points, respectively. While the data were collected in an imaging experiment, it has been presented as in aggregate owing to the complexity of the data. It should be appreciated that such a cube of data (*a*) would be available for each spatial position. The T-8883 beads are 1 µm polystyrene microspheres containing a proprietary mix of dyes. In (*a*), the dominant feature is the cloud of points running approximately parallel to the wavelength axis. This portion of the data corresponds to the later time points and wavelengths between 540 and 650 nm and is centred near (0.23 and 0.27) when projected onto the (*B*, *A*) plane. This portion of the dataset has been highlighted. The region at the top primarily represents the terminal acceptor at early time intervals in the 2 hour experiment. Data adapted from Hanley *et al.* (2006).

AB-space to move around the semicircle (figure 4). In the context of SFLIM, figure 4 is important as it suggests that 80 MHz is possibly the best of the three shown for resolving two fluorophores having lifetimes of 1 and 5 ns by methods relying on α. This conclusion may be reached by noting that the line segment connecting the two fluorophores is the longest at 80 MHz. This indicates that at 80 MHz, a change in α will produce the largest change in position along the line segment connecting the two. This conclusion is independent of whether α varies with position or wavelength. Similar considerations can be used when selecting fluorophores.

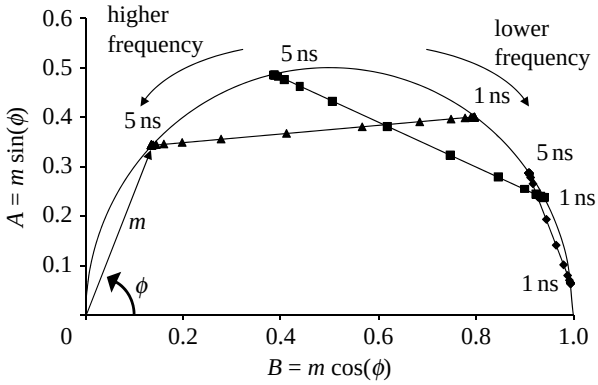

Figure 4. Frequency-dependent polar plot of a simulation of a mixture of two fluorophores having lifetimes of 1 and 5 ns at three frequencies 10 (diamonds), 40 (squares) and 80 (triangles) MHz presented in the *AB*-format. The locations of the pure lifetime components have been highlighted to show the trajectory along the arc of the semicircle. A vector has been added to illustrate the relationship between m and ϕ and the *AB*-position for the pure 5 ns component measured at 80 MHz.

2.7. Single-step energy transfer

SFLIM provides a unique opportunity to study energy transfer through the simultaneous observation of the donor and acceptor. Energy transfer is a rate process competing with the rate of donor emission, k_D.[3]

$$k_{DA} = k_{FRET} + k_D \quad \text{and} \quad \tau_{DA} = \frac{1}{k_{DA}}, \tag{2.10}$$

$$E = \frac{k_{FRET}}{k_{FRET} + k_D}, \tag{2.11}$$

where k_{DA} is the rate of donor emission in the presence of an acceptor; k_D is the rate of donor emission in the absence of the acceptor; k_{FRET} is the rate of energy transfer; and E is the energy transfer efficiency. The rate of energy transfer k_{FRET} depends on the distance r, between the donor and acceptor and the Forster radius R_0 (cf. Valeur 2002).

$$k_{FRET} = k_D \left(\frac{R_0}{r}\right)^6. \tag{2.12}$$

Assuming that in the absence of the acceptor the only process depopulating the excited state is the radiative rate, this expression indicates that when r is equal to R_0, $k_{FRET} = k_D$. In other words, if such a fluorophore has a fluorescence lifetime of 4 ns, the rate of donor emission will be $2.5 \times 10^8\ s^{-1}$. In the presence of an acceptor located at the Forster radius, this results in $k_{FRET} = 2.5 \times 10^8\ s^{-1}$ as well. Following equations (2.10)–(2.12), the observed lifetime of the donor in this donor–acceptor complex will then be 2 ns.

2.8. Multistep energy transfer

In cases where the acceptor is excited through a donor or a multistep donor–acceptor series, a set of simple rules applies (Lakowicz & Balter 1982*a*,*b*). For a

[3]For simplicity of treatment, only two processes are considered here: radiative release of energy as a photon and energy transfer.

multistep energy transfer process, the phase angle for the nth step is given by the sum of the phase angles of each step. The modulation depth of the fluorescence from the nth step is the product of the modulation depths.

$$\phi_n = \sum_{i=1}^{n} \phi_i \tag{2.13}$$

and

$$m_n = \prod_{i=1}^{n} m_i, \tag{2.14}$$

where ϕ_i and m_i are the phase angle and modulation depth, respectively, for the ith fluorophore. Allowed values of ϕ_i are between 0 and 90° (0–$\pi/2$ radians), and m_i are between 0 and 1. For single components, ϕ_i and m_i may be computed by rearranging equations (2.1) and (2.2).[4]

$$\phi_i = \tan^{-1}(\omega\tau_i) \tag{2.15}$$

and

$$m_i = \sqrt{\frac{1}{1+\omega^2\tau_i^2}}. \tag{2.16}$$

2.9. Predicting donor, donor in the presence of acceptor, acceptor and acceptor in the presence of the donor in the case of single-step energy transfer

Equations (2.10)–(2.16) may be employed to predict the main components of a donor–acceptor system (figure 5). A sample containing a pair of fluorophores forming a putative donor–acceptor pair when in close proximity may contain free donor, donor in the presence of acceptor, free acceptor and acceptor excited through the donor via energy transfer. The range of possible results from such a system may be predicted in four steps (figure 5):

(i) Compute the modulation depth and phase for the donor (m_D and ϕ_D) and acceptor (m_A and ϕ_A) at the modulation frequency using equations (2.15) and (2.16). In figure 5, the modulation frequency is 60 MHz, the donor lifetime is 4 ns and the acceptor lifetime is 5 ns.

(ii) Compute the rate constants k_D and k_{FRET} (in figure 5, these are assumed to be equal). Add the two rate constants and compute τ_{DA} using equation (2.10). Use equations (2.15) and (2.16) to obtain m_{DA} and ϕ_{DA}. The modulation and phase of the acceptor in the presence of the donor (m_{AD} and ϕ_{AD}) can now be computed by adding ϕ_{DA} and ϕ_A (equation (2.13)) and multiplying m_{DA} by m_A (equations (2.14)).

(iii) Convert the values of m and ϕ to AB-coordinates using equations (2.7) and (2.8) and plot these in the AB-space.

(iv) The polygon formed by the four points is the boundary of all possible results from a system consisting of a single donor–acceptor pair.

[4]For brevity, x, y, z and λ have been dropped from these equations.

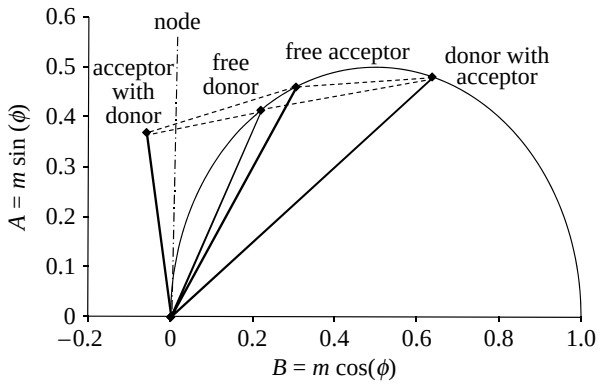

Figure 5. AB-space simulation of a donor–acceptor system consisting of two fluorophores. Specifications for the simulation: donor lifetime (4 ns), acceptor lifetime (5 ns), donor–acceptor separated by the Forster radius (rate of energy transfer equal to the radiative rate) and frequency of modulation 60 MHz. The position of the vertical dot-dashed line indicates the position of a node. Measured values of the phase will generate ill-behaved phase lifetimes at this location if propagated through equation (2.1). To the left of the node, negative phase lifetimes are generated.

What should be noted in this case is that the range of values generated by this system cannot be presented as traditional lifetimes owing to the behaviour of the tangent function. The alternative presentation of modulation and phase in polar coordinates is invaluable when both the donor and acceptor regions of the spectrum are observed using frequency-domain methods.

2.10. Very efficient energy transfer

A special case exists when energy transfer is very efficient (Forde & Hanley 2006). Under these conditions, the donors in the donor–acceptor complex will emit little or no light and the values of ϕ_i approach 0 and m_i approach 1 for all but the terminal acceptor in a series. This final acceptor exhibits no observable change in lifetime parameters. A worst-case scenario is a donor–acceptor system consisting of free donor (exhibiting its normal lifetime), free acceptor (exhibiting its normal lifetime) and donor–acceptor complex with highly efficient energy transfer (exhibiting the normal lifetime of the acceptor).[5] Such a scenario is unlikely in biological systems due to the size of the molecules involved, but is quite realistic in a variety of chemical systems. One way to probe such a system would be an acceptor photobleaching experiment in which the variations in the intensity of the donor and acceptor are observed. In the presence of energy transfer, signal from the donor should increase when the acceptor is photobleached.

2.11. Energy transfer and AB-space measurements lying on the semicircle

Many treatments of the AB-plots rest on the assumption of two non-interacting fluorophores (Clayton *et al.* 2004; Hanley & Clayton 2005). The standard approach

[5]This may be tested by following the scenario in figure 5 except making k_{FRET} 100 times k_D.

is to fit a line in the AB-space to a set of points,

$$A_i = u + vB_i. \tag{2.17}$$

From the intercept u and slope v of the straight line, the component lifetimes may be computed via equation (2.9).

This approach works only if there is no acceptor signal present in the data. SFLIM allows both the donor and acceptor to be observed, which undercuts this assumption. In the AB-coordinates, sample heterogeneity in non-interacting species tends to move the measured data into the semicircle, while acceptor signals and excited-state reactions tend to push the resulting data outside (cf. figure 5). There are many scenarios in which energy transfer can cause a system to cross and recross the semicircle in an AB-plot (cf. figures 6 and 7 (below)). Therefore, if it is suspected that the acceptor signals are a component of a measured dataset, equation (2.9) should be used cautiously and the appearance of the data lying on the semicircle of an AB-plot should not be interpreted as a proof of a single lifetime (Forde & Hanley 2006).

2.12. *Energy transfer and allowed regions in AB*-space

The accessibility of acceptor signals in SFLIM present special data presentation problems. The conditions modelled in figure 5 are such that the phase lifetimes cannot be presented at the point where $B=0$. This occurs when the phase is 90°, which results in an undefined phase lifetime. Such conditions are realistic when observing portions of the spectrum containing acceptor emission. For example, Forde (2005) measured SFLIM parameters on samples exhibiting multistep energy transfer (figure 6). The experimental data clearly cross the node (where $B=0$ in figure 6*a*) and also exhibited a very striking excursion into the lower right-hand quadrant of the AB-space (figure 6*b*,*c*). The data were collected at a time (2004) when it was assumed that the points should always lie within the semicircle and above the x-axis. As such, the data were initially looked at sceptically as there was no clear explanation. The data showed a clear evolution with time, but no simple model of single-step energy transfer was able to replicate the basic trends. These data raised a question: what portion of AB-space is 'allowed' and what is 'forbidden'?

The work of Lakowicz & Balter (1982*a*,*b*) and its translation into the AB-space (Forde 2005; Forde & Hanley 2006) provide a foundation to both understand the trends seen in figure 6 and to determine which portions of the AB-space are allowed. This question can be answered by noting that the energy transfer efficiency is bounded at 1 (equation (2.11)). Molecules excited through an energy transfer series will eventually become too dim to observe. For example, if the rate of energy transfer is equal to the radiative rate and no dark processes compete, the number of photons observed from the donor and acceptor should, to a first approximation, be equal.

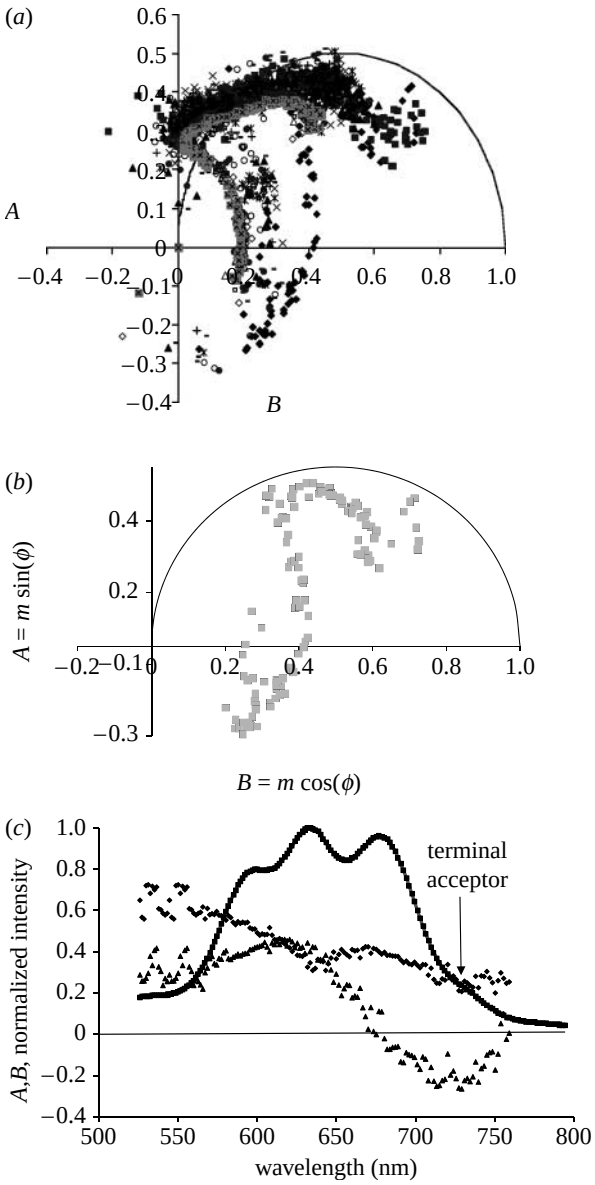

Figure 6. An AB-plot of the SFLIM data collected while photobleaching Molecular Probes T-8869 fluorescent 40 nm microspheres with primarily the 546 nm line of a Hg arc lamp. The T-8869 beads consist of a system of six BODIPY dyes emitting at 720, 678, 635, 592, 560 and 515 nm. Under normal conditions, these microspheres exhibit highly efficient energy transfer along a series beginning with the first donor (515 nm) to the terminal acceptor (720 nm) (Roberts *et al.* 1998; Forde & Hanley 2005). Bleaching with the 546 nm line of Hg disrupts the energy transfer series. (*a*) All data from a photobleaching experiment measured at 10 min intervals over a 2 hour period (filled diamonds, 0 min; filled squares, 10 min; filled triangles, 20 min; crosses, 30 min; asterisks, 40 min; filled circles, 50 min; pluses, 60 min; minuses, 70 min; open circles, 80 min; open diamonds, 90 min; open squares, 100 min; open triangles, 110 min; shaded crosses, 120 min; thin solid curve, half circle). Adapted with permission from Forde (2005). As noted in figure 3, data from an imaging experiment have been presented in aggregate owing to the complexity of the data. The data in (*a*) would be available for each spatial position. (*b*) Initial time point showing the frequency-domain data in the AB-space. These data and the data shown in (*a*) clearly show the population of the lower right quadrant. (*c*) Intensity (squares), A (triangles) and B (diamonds) plotted with wavelength. These data highlight the consistent trend with wavelength.

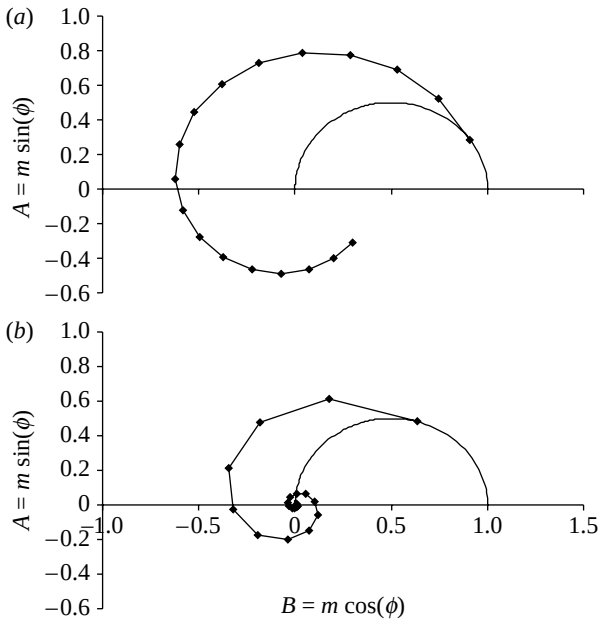

Figure 7. Allowed regions of the *AB*-space. (*a*) Simulation of a multistep process in which each species has a 20 ns lifetime, the distance between the donor and acceptor results in 75% energy transfer efficiency and the modulation frequency is 10 MHz. This yields an observed 5 ns lifetime for each species. With 75% energy transfer, the intensity will fall below 1% by the 18th transfer step. (*b*) Simulation of a multistep energy transfer process in which each species has a 4 ns lifetime, the acceptor is placed one Forster radius from the donor, and the modulation frequency is set to 60 MHz. This yields an observed donor lifetime for each species of 2 ns. Note: by the 7th step, the observed intensity will have fallen to less than 1% of the first donor.

The assumption of no competing dark processes is equivalent to assuming that the quantum yields of both the donor and acceptor are 1. If the acceptor transfers 50 per cent of its energy via FRET to a subsequent acceptor then the amount of light observed from the first acceptor will be one-half of that from the principal donor. The amount of light observed from the ith acceptor is therefore related to the product of the energy transfer efficiencies from the principal donor in the absence of an acceptor.

Equations (2.7), (2.8) and (2.10)–(2.14) allow the calculation of the *AB*-positions of a system of fluorophores undergoing multistep energy transfer (figure 7). Consider a set of fluorophores undergoing energy transfer, all of which have the same lifetime and all positioned one Forster radius away from the next fluorophore in the energy transfer series. Under these conditions, the multistep process follows a trajectory around the coordinate system visiting all quadrants (figure 7*a*). These simulations indicate that the allowed region of the *AB*-space is a unit circle centred on the origin. By careful selection of the modulation frequency and system characteristics, any point within the unit circle may be populated. Most such systems are experimentally unlikely; more realistic scenarios consist of a spiral rapidly converging on the origin (figure 7*b*). The data in the lower quadrants are likely to be rare but are indeed possible (figure 6). There is, however, no way to reach the lower quadrants with a single-step excited-state process.[6] Energy transfer between a single donor–acceptor pair is a single-step process and would not be expected to ever appear in the lower quadrants.

3. CONCLUSION

SFLIM is a tool allowing multiple fluorescent species in a sample to be observed. Its greatest success has been in looking at model systems with multiple energy transfer steps. The future of the method depends on the development of better data analysis tools allowing non-specialists to make use of it, particularly in biological applications. This, in turn, has driven the exploration of data presentation. Because SFLIM is well suited to observing acceptors, general issues in the presentation of frequency-domain lifetime images have been highlighted. In particular, the lifetime computed from the measured phase in a frequency-domain experiment can be ill behaved when looking at an acceptor. When the phase approaches 90°, the phase lifetime approaches infinity. As soon as it passes 90°, it immediately switches to large negative values. The underlying theory of this effect has been available for some time (Lakowicz & Balter 1982*a*,*b*), but the consequences are not widely appreciated because acceptors are rarely observed in FLIM studies. Widely used data presentation practices, such as clipping lifetime images at 0, will systematically remove useful and informative data. The *AB*-presentation completely solves this problem of ill behaviour.

As a technique, many opportunities and challenges remain before SFLIM is widely used. Some of the challenges remain quite basic: selection of fluorophores; automation of data analysis; presentation of the data; and optimal experimental design. This review has tried to highlight where open questions remain. The opportunities are great. One of the earliest examples of FD-SFLIM included biological specimens, the key parts of which are found in figure 8. Since then, relatively few studies have applied SFLIM to cell biology and there remains considerable scope for pioneering work in this area. For example, applying global analysis (Verveer *et al.* 2000) to the data from both the donor and the acceptor in a scheme that includes wavelength-dependent frequency-domain data and conventional intensity spectra could assist in discerning proximity relationships. This could be further refined to multiple donor multiple acceptor systems. Such a capability is not currently available. Another example is combinatorial labelling. This approach has for some years found success combined with imaging spectroscopy to perform, e.g. spectral karyotyping (Garini *et al.* 1996). Briefly, the method uses the presence or absence of n dyes to label 2^n-1 objects. With three dyes, five objects can be uniquely labelled. With SFLIM, more information could be extracted from those five objects or the same three dyes could label more objects.

[6]The maximum phase a single fluorophore may exhibit is 90°. The sum of two such phase shifts (equation (2.13)) is 180°. All single-step processes are therefore restricted to the two quadrants having positive A values.

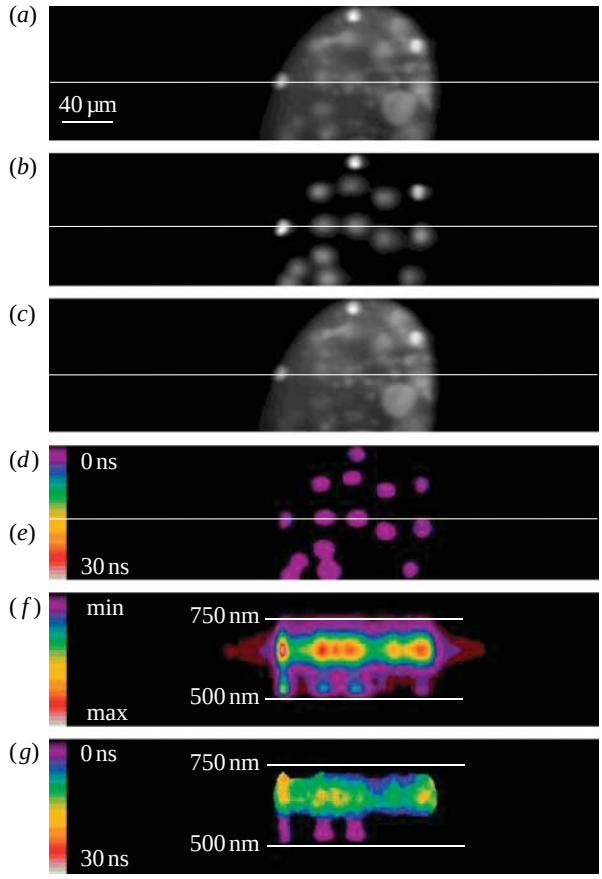

Figure 8. *Drosophila* salivary gland explant expressing an EGFP histone and stained with PI. This set of images illustrates the power of SFLIM. Images show (*a*) a sum over all wavelengths, (*b*) an intensity slice at 518 nm showing the localization of EGFP, (*c*) an intensity slice at 615 showing the distribution of PI, (*d*) modulation lifetime image at 518 nm (0 ns), (*e*) modulation lifetime image at 615 nm (30 ns), (*f*) intensity spectral image and (*g*) lifetime spectral image. The line running across (*a–d*) corresponds to the position of the spectral images in (*f*) and (*g*). Data adapted from Hanley *et al.* (2002).

Projecting into the future, a number of applications can be envisioned. These include going beyond the dominant paradigm of single donor single acceptor studies viewed at donor wavelengths to allow imaging of multiple protein–protein interactions. Multiparameter imaging with SFLIM should be uniquely suited to studying complex photophysics, photochemistry and photobiology. For example, it could be used to expand the understanding of the photophysics of intact corals (Hanley *et al.* 2006) an area that is relatively little studied. Other examples might include applications in functional proteomics, drug screening and multiplexed diagnostics.

Support for this work comes from the Engineering and Physical Sciences Research Council under a Life Science Interface Grant EP/E013422/1 and the European Union Sixth Framework Program as part of the FLUOROMAG consortium under contract no. 037465. The author wishes to thank Prof. Kaminski for the invitation to speak in this series of lectures, Lambert Instruments for sponsoring his talk, and Dr Yanzhou Zhou for MATLAB assistance in replotting the data found in figure 3.

REFERENCES

Bird, D. K., Eliceiri, K. W., Fan, C. H. & White, J. G. 2004 Simultaneous two-photon spectral and lifetime fluorescence microscopy. *Appl. Opt.* **43**, 5173–5182. (doi:10.1364/AO.43.005173)

Clayton, A. H. A., Hanley, Q. S. & Verveer, P. J. 2004 Graphical representation and multicomponent analysis of single-frequency fluorescence lifetime imaging microscopy data. *J. Microsc.* **213**, 1–5. (doi:10.1111/j.1365-2818.2004.01265.x)

Colyer, R. A., Lee, C. & Gratton, E. 2008 A novel fluorescence lifetime imaging system that optimizes photon efficiency. *Microsc. Res. Tech.* **71**, 201–213. (doi:10.1002/jemt.20540)

De Beule, P. *et al.* 2007 Rapid hyperspectral fluorescence lifetime imaging. *Microsc. Res. Tech.* **70**, 481–484. (doi:10.1002/jemt.20434)

Digman, M. A., Caiolfa, V. R., Zamai, M. & Gratton, E. 2008 The phasor approach to fluorescence lifetime imaging analysis. *Biophys. J.* **94**, L14–L16. (doi:10.1529/biophysj.107.120154)

Dinish, U. S., Fu, C. Y., Chao, Z. X., Seah, L. K., Murukeshan, V. M. & Ng, B. K. 2006 Subnanosecond-resolution phase-resolved fluorescence imaging technique for biomedical applications. *Appl. Opt.* **45**, 5020–5026. (doi:10.1364/AO.45.005020)

Elder, A. D., Matthews, S. M., Swartling, J., Yunas, K., Frank, J. H., Brennan, J. D., Fisher, A. C. & Kaminski, C. F. 2006 The application of frequency-domain fluorescence lifetime imaging microscopy as a quantitative analytical tool for microfluidic devices. *Opt. Express* **14**, 5456–5467. (doi:10.1364/OE.14.005456)

Esposito, A., Gerritsen, H. C. & Wouters, F. S. 2005 Fluorescence lifetime heterogeneity resolution in the frequency domain by lifetime moment analysis. *Biophys. J.* **89**, 4286–4299. (doi:10.1529/biophysj.104.053397)

Forde, T. S. 2005 Determination of fluorescence resonance energy transfer in multi-fluorophore systems: theoretical and experimental analysis. In *Department of biological and chemical sciences*, vol. M. Phil.: University of the West Indies.

Forde, T. S. & Hanley, Q. S. 2005 Following FRET through five energy transfer steps: spectroscopic photobleaching, recovery of spectra, and a sequential mechanism of FRET. *Photochem. Photobiol. Sci.* **4**, 609–616. (doi:10.1039/b416478d)

Forde, T. S. & Hanley, Q. S. 2006 Spectrally resolved frequency domain analysis of multi-fluorophore systems undergoing energy transfer. *Appl. Spectrosc.* **60**, 1442–1452. (doi:10.1366/000370206779321544)

Gadella Jr, T. W. J., Clegg, R. M. & Jovin, T. M. 1994 Fluorescence lifetime imaging microscopy: pixel-by-pixel analysis of phase-modulation data. *Bioimaging* **2**, 139–159. (doi:10.1002/1361-6374(199409)2:3<139::AID-BIO4>3.3.CO;2-K)

Garini, Y. *et al.* 1996 Spectral karyotyping. *Bioimaging* **4**, 65–72. (doi:10.1002/1361-6374(199606)4:2<65::AID-BIO4>3.3.CO;2-4)

Hanley, Q. S. & Clayton, A. H. A. 2005 *AB*-plot assisted determination of fluorophore mixtures in a fluorescence lifetime microscope using spectra or quenchers. *J. Microsc.* **218**, 62–67. (doi:10.1111/j.1365-2818.2005.01463.x)

Hanley, Q. S. & Ramkumar, V. 2005 An internal standardization procedure for spectrally resolved fluorescence lifetime imaging (sFLIM). *Appl. Spectrosc.* **59**, 261–266. (doi:10.1366/0003702053085142)

Hanley, Q. S., Verveer, P. J. & Jovin, T. M. 1999 Spectral imaging in a programmable array microscope by Hadamard transform fluorescence spectroscopy. *Appl. Spectrosc.* **53**, 1–10. (doi:10.1366/0003702991945317)

Hanley, Q. S., Verveer, P. J., Arndt-Jovin, D. J. & Jovin, T. M. 2000 Three-dimensional spectral imaging by Hadamard transform spectroscopy in a programmable array microscope. *J. Microscopy-Oxford* **197**, 5–14. (doi:10.1046/j.1365-2818.2000.00665.x)

Hanley, Q. S., Subramaniam, V., Arndt-Jovin, D. J. & Jovin, T. M. 2001 Fluorescence lifetime imaging: multipoint calibration, minimum resolvable differences, and artifact suppression. *Cytometry* **43**, 248–260. (doi:10.1002/1097-0320(20010401)43:4<248::AID-CYTO1057>3.0.CO;2-Y)

Hanley, Q. S., Arndt-Jovin, D. J. & Jovin, T. M. 2002 Spectrally resolved fluorescence lifetime imaging microscopy. *Appl. Spectrosc.* **56**, 155–166. (doi:10.1366/0003702021954610)

Hanley, Q. S., Lidke, K. A., Heintzmann, R., Arndt-Jovin, D. J. & Jovin, T. M. 2005 Fluorescence lifetime imaging in an optically sectioning programmable array microscope (PAM). *Cytometry A* **67A**, 112–118. (doi:10.1002/cyto.a.20177)

Hanley, Q. S., Murray, P. I. & Forde, T. S. 2006 Microspectroscopic fluorescence analysis with prism-based imaging spectrometers: review and current studies. *Cytometry A* **69A**, 759–766. (doi:10.1002/cyto.a.20265)

Jameson, D. M., Gratton, E. & Hall, R. D. 1984 The measurement and analysis of heterogeneous emissions by multifrequency phase and modulation fluorometry. *Appl. Spectrosc. Rev.* **20**, 55–106. (doi:10.1080/05704928408081716)

Jones, C. R., Bolton, P. H. & Kearns, D. R. 1978 Ethidium-bromide binding to transfer-RNA—transfer-RNA as a model system for studying drug-RNA interactions. *Biochemistry* **17**, 601–607. (doi:10.1021/bi00597a007)

Knemeyer, J. P., Herten, D. P. & Sauer, M. 2003 Detection and identification of single molecules in living cells using spectrally resolved fluorescence lifetime imaging microscopy. *Anal. Chem.* **75**, 2147–2153. (doi:10.1021/ac026333r)

Knemeyer, J. P., Marme, N. & Hoheisel, J. D. 2007 Spectrally resolved fluorescence lifetime imaging microscopy (SFLIM)—an appropriate method for imaging single molecules in living cells. *Anal. Bioanal. Chem.* **387**, 37–40. (doi:10.1007/s00216-006-0762-1)

Lakowicz, J. R. 1999 *Principles of fluorescence spectroscopy.* pp. 142–184. New York, NY: Kluwer Academic/Plenum Publishers.

Lakowicz, J. R. & Balter, A. 1982*a* Analysis of excited-state processes by phase-modulation fluorescence spectroscopy. *Biophys. Chem.* **16**, 117–132. (doi:10.1016/0301-4622(82)85013-8)

Lakowicz, J. R. & Balter, A. 1982*b* Theory of phase-modulation fluorescence spectroscopy for excited-state processes. *Biophys. Chem.* **16**, 99–115. (doi:10.1016/0301-4622(82)85012-6)

Leupin, W., Feigon, J., Denny, W. A. & Kearns, D. R. 1985 Substituent effects on the binding of ethidium and its derivatives to natural DNA. *Biophys. Chem.* **22**, 299–305. (doi:10.1016/0301-4622(85)80053-3)

Levenson, R. M. 2006 Spectral imaging perspective on cytomics. *Cytometry* **69A**, 592–600. (doi:10.1002/cyto.a.20292)

Marriott, G., Clegg, R. M., Arndt-Jovin, D. J. & Jovin, T. M. 1991 Time resolved imaging microscopy—phosphorescence and delayed fluorescence imaging. *Biophys. J.* **60**, 1374–1387.

Olmsted, J. & Kearns, D. R. 1977 Mechanism of ethidium-bromide fluorescence enhancement on binding to nucleic-acids. *Biochemistry* **16**, 3647–3654. (doi:10.1021/bi00635a022)

Pelet, S., Previte, M. J. R., Kim, D., Kim, K. H., Su, T. T. J. & So, P. T. C. 2006 Frequency domain lifetime and spectral imaging microscopy. *Microsc. Res. Tech.* **69**, 861–874. (doi:10.1002/jemt.20361)

Redford, G. I. & Clegg, R. M. 2005 Polar plot representation for frequency-domain analysis of fluorescence. *J. Fluoresc.* **15**, 805–815. (doi:10.1007/s10895-005-2990-8)

Roberts, D. V., Wittmershaus, B. P., Zhang, Y. Z., Swan, S. & Klinowsky, M. P. 1998 Efficient excitation energy transfer among multiple dyes in polystyrene microspheres. *J. Luminescence* **79**, 225–231. (doi:10.1016/S0022-2313(98)00044-1)

Rück, A., Hülshoff, C., Kinzler, I., Becker, W. & Steiner, R. 2007 SLIM: a new method for molecular imaging. *Microsc. Res. Tech.* **70**, 485–492. (doi:10.1002/jemt.20433)

Schneider, P. C. & Clegg, R. M. 1997 Rapid acquisition, analysis, and display of fluorescence lifetime-resolved images for real-time applications. *Rev. Sci. Instrum.* **68**, 4107–4119. (doi:10.1063/1.1148354)

Spencer, R. D. & Weber, G. 1969 Measurements of subnanosecond fluorescence lifetimes with a cross-correlation phase fluorometer. *Ann. N Y Acad. Sci.* **158**, 361–376. (doi:10.1111/j.1749-6632.1969.tb56231.x)

Squire, A., Verveer, P. J. & Bastiaens, P. I. H. 2000 Multiple frequency fluorescence lifetime imaging microscopy. *J. Microsc.-Oxford* **197**, 136–149. (doi:10.1046/j.1365-2818.2000.00651.x)

Tinnefeld, P., Herten, D. P. & Sauer, M. 2001 Photophysical dynamics of single molecules studied by spectrally-resolved fluorescence lifetime imaging microscopy (SFLIM). *J. Phys. Chem. A* **105**, 7989–8003. (doi:10.1021/jp010365l)

Tramier, M., Kemnitz, K., Durieux, C. & Coppey-Moisan, M. 2004 Picosecond time-resolved microspectrofluorometry in live cells exemplified by complex fluorescence dynamics of popular probes ethidium and cyan fluorescent protein. *J. Microsc.* **213**, 110–118. (doi:10.1111/j.1365-2818.2004.01271.x)

Valeur, B. 2002 *Molecular fluorescence principles and applications.* Weinheim, Germany: WILEY-VCH Verlag GmbH.

Vereb, G., Jares-Erijman, E., Selvin, P. R. & Jovin, T. M. 1998 Temporally and spectrally resolved imaging microscopy of lanthanide chelates. *Biophys. J.* **74**, 2210–2222.

Verveer, P. J. & Bastiaens, P. I. H. 2003 Evaluation of global analysis algorithms for single frequency fluorescence lifetime imaging microscopy data. *J. Microsc.* **209**, 1–7. (doi:10.1046/j.1365-2818.2003.01093.x)

Verveer, P. J., Squire, A. & Bastiaens, P. I. H. 2000 Global analysis of fluorescence lifetime imaging microscopy data. *Biophys. J.* **78**, 2127–2137.

Weber, G. 1981 Resolution of the fluorescence lifetimes in a heterogeneous system by phase and modulation measurements. *J. Phys. Chem.* **85**, 949–953. (doi:10.1021/j150608a006)

Yan, L., Rueden, C. I., White, J. G. & Eliceiri, K. W. 2006 Applications of combined spectral lifetime microscopy for biology. *Biotechniques* **41**, 249–257. (doi:10.2144/000112251)